

Improving global scale land cover classifications with multi-directional POLDER data and a decision tree classifier

Eric C. Brown de Colstoun^{a,*}, Charles L. Walthall^b

^a Science Systems and Applications, Inc., Code 614.4, Biospheric Sciences Branch, NASA/Goddard Space Flight Center, Greenbelt, MD 20771, USA

^b Hydrology and Remote Sensing Laboratory, USDA Agricultural Research Service, Beltsville, MD, USA

Received 14 April 2005; received in revised form 10 November 2005; accepted 12 November 2005

Abstract

Several investigations indicate that the Bidirectional Reflectance Distribution Function (BRDF) contains information that can be used to complement spectral information for improved land cover classification accuracies. Prior studies on the addition of BRDF information to improve land cover classifications have been conducted primarily at local or regional scales. Thus, the potential benefits of adding BRDF information to improve *global* to continental scale land cover classification have not yet been explored. Here we examine the impact of multidirectional global scale data from the first Polarization and Directionality of Earth Reflectances (POLDER) spacecraft instrument flown on the Advanced Earth Observing Satellite (ADEOS-1) platform on overall classification accuracy and per-class accuracies for 15 land cover categories specified by the International Geosphere Biosphere Programme (IGBP).

A set of 36,648 global training pixels (7×6 km spatial resolution) was used with a decision tree classifier to evaluate the performance of classifying POLDER data with and without the inclusion of BRDF information. BRDF 'metrics' for the eight-month POLDER on ADEOS-1 archive (10/1996–06/1997) were developed that describe the temporal evolution of the BRDF as captured by a semi-empirical BRDF model. The concept of BRDF 'feature space' is introduced and used to explore and exploit the bidirectional information content. The C5.0 decision tree classifier was applied with a boosting option, with the temporal metrics for spectral albedo as input for a first test, and with spectral albedo and BRDF metrics for a second test. Results were evaluated against 20 random subsets of the training data.

Examination of the BRDF feature space indicates that coarse scale BRDF coefficients from POLDER provide information on land cover that is different from the spectral and temporal information of the imagery. The contribution of BRDF information to reducing classification errors is also demonstrated: the addition of BRDF metrics reduces the mean, overall classification error rates by 3.15% (from 18.1% to 14.95% error) with larger improvements for producer's accuracies of individual classes such as Grasslands (+8.71%), Urban areas (+8.02%), and Wetlands (+7.82%). User's accuracies for the Urban (+7.42%) and Evergreen Broadleaf Forest (+6.70%) classes are also increased. The methodology and results are widely applicable to current multidirectional satellite data from the Multi-angle Imaging Spectroradiometer (MISR), and to the next generation of POLDER-like multi-directional instruments.

© 2005 Elsevier Inc. All rights reserved.

Keywords: Global land cover; BRDF; Decision tree

1. Introduction

Land cover and land use are principal factors, in both space and time, controlling the cycling and exchange of carbon, energy and water within, and between, the different Earth systems. Thus, global land cover classifications are essential for a variety of diagnostic and predictive models that simulate

the functioning of the Earth systems and are useful for investigating global change (Sellers et al., 1996; Townshend et al., 1994). Global land cover classifications also simplify the monitoring of natural or human-induced changes of land cover/use and are important in simulations of the *impact* of such changes on local and global processes (e.g. Bonan, 1997; Bounoua et al., 2002). In addition, coarse scale land cover classifications currently play an important role as ancillary data for various parameter retrieval algorithms using data from the *Terra* and *Aqua* satellite systems, and are expected to be used by several of the algorithms of the future National Polar

* Corresponding author. Tel.: +1 301 614 6597; fax: +1 301 614 6695.

E-mail address: ericbdc@ltpmail.gsfc.nasa.gov (E.C. Brown de Colstoun).

Orbiting Environmental Satellite System (NPOESS) Preparatory Project (NPP) and the NPOESS operational satellite systems, to be launched later this decade and early next decade, respectively.

Global scale land cover classifications derived from Advanced Very High Resolution Radiometer (AVHRR) satellite data have achieved accuracies between 70% and 90% for up to 17 land cover types. Classifications using 8 km or coarser resolutions yield accuracies over 80% (DeFries et al., 1995, 1998; Friedl & Brodley 1997; Hansen et al., 1996), and those using 1 km resolution data yield accuracies near 70% (Hansen et al., 2000; Scepán, 1999). These classification accuracies in some cases have been determined from random samples of unseen test cases taken from samples used to train the classifier (DeFries et al., 1995, 1998; Friedl & Brodley, 1997; Hansen et al., 2000). Thus, actual accuracies can be expected to be lower when tested with independent validation data, as shown by Friedl et al. (2000). The correct typing probability for the 1 km IGBP-DIScover global land cover classification of Loveland and Belward (1997), checked against such an independent validation data set, was expected to reach 85%, but is in fact 67% (Scepán, 1999). The land cover product from the MODerate Resolution Imaging Spectroradiometer (MODIS) (Friedl et al., 2002; Strahler et al., 1999) is expected to have an accuracy near 80%.

The limitations to achieving higher classification accuracies discussed by DeFries et al. (1998), Loveland et al. (1999), and Hansen et al. (2000), emphasize data quality of the input data and the number and nature of the land cover classes of interest. Artifacts of data processing, substantial radiometric noise, geolocation errors, and the limited spectral coverage of systems such as AVHRR inhibit the ability to separate spectrally similar land cover classes. Many land cover types, especially at coarse spatial scales, show as much intra-class variability as inter-class spectral variability. This variability frequently exhibits multimodal distributions that cause serious difficulties for traditional classifiers such as Maximum Likelihood Classifiers (MLC). New non-parametric classifiers such as decision trees are preferred to parametric classifiers for coarse resolution applications because these do not assume normally distributed input data, as a MLC does (Friedl & Brodley, 1997; Hansen et al., 1996).

Improved classifications should also result from improved processing of the input data such as atmospheric corrections and may also benefit from mitigation of the non-Lambertian behavior of terrestrial surfaces. The data currently available from sensors such as MODIS, and the Visible/Infrared Imager/Radiometer Suite (VIIRS) to be flown onboard NPP and NPOESS, incorporate such corrections and (will) have significantly superior radiometric performance and stability. Additional spectral bands, particularly in the middle infrared portion of the spectrum, and improved geolocation are also expected to substantially benefit land cover classification algorithms and any derived products.

Principal sources of confusion for global scale classifications are usually absent between large ‘core’ classes such as forest and bare/sparsely vegetated (e.g. DeFries et al., 1998;

Han et al., 2004; Hansen & Reed, 2000). Confusion typically occurs between surfaces that are similar spectrally and temporally, such as different forest types (e.g. Deciduous Broadleaf Forest and Mixed Forest), Wooded Grasslands and Woodlands, Open and Closed Shrublands, and/or Grasslands and Croplands. In addition, other classes such as Urban areas and Wetlands are poorly characterized from visible/infrared satellite data (Han et al., 2004; Scepán, 1999).

Ancillary information, or orthogonal information such as surface structure or polarization, may be useful for reducing errors currently encountered with the use of spectral/temporal data alone. Investigations of the bidirectional reflectance distribution function (BRDF) suggest that multi-angular signatures contain information on land cover surface structure unavailable from nadir or near-nadir spectral signatures (Bicheron & Leroy, 2000; Deering et al., 1999; Irons et al., 1992; Kimes et al., 1985; Kriebel, 1978; Pinty et al., 2002; Walthall & Brown de Colstoun, 1997). Most multi-angular studies have been carried out at the local, plot-level scale and thus have not examined the variability of BRDF across landscapes at coarse spatial scales. It is suggested that the vertical structure of global land cover types, and the associated shadowing of canopy or surface components caused by this vertical structure are associated with land cover and when parameterized by simple semi-empirical BRDF models can be used to improve global land cover classifications. The research presented here addresses information content of global scale BRDF signatures with respect to land cover type. The potential of global BRDF patterns as an aid to the discrimination of land cover types is evaluated using eight months of global multi-directional data acquired by the first Polarization and Directionality of Earth Reflectances (POLDER) satellite, processed and provided by the Centre National d’Études Spatiales (CNES), Toulouse, France. The coefficients of the semi-empirical Roujean et al. (1992) BRDF kernel model are used as a basis for multi-directional ‘metrics’ describing the evolution of the BRDF for 15 IGBP land cover types for the entire eight-month POLDER archive. By assessing the spectral and temporal POLDER data alone, and then including the BRDF metrics along with the spectral and temporal data in a second test, the contributions of BRDF information to global land cover classifications in terms of overall, and individual IGBP class accuracy, are examined. This analysis is facilitated by the use of a commercially available non-parametric decision tree classifier called C5.0 (Quinlan, 1993).

2. Background

2.1. Global land cover classifications and decision trees

Current global land cover products generated from MODIS data (Friedl et al., 2002) follow the heritage of previous work with AVHRR data (DeFries et al., 1998; Hansen et al., 2000), particularly in terms of the decision tree classifiers and the use of training data derived from Landsat Thematic Mapper (TM) and/or Enhanced Thematic Mapper Plus (ETM+). A decision tree classifier approach following this AVHRR/MODIS heri-

tage is currently planned for the operational land cover products to be produced from the VIIRS sensor onboard NPP and NPOESS (Brown de Colstoun et al., 2000). Decision trees are becoming popular for these coarse-scale applications because they do not make any implicit assumptions about normal distributions in the training data, as some more traditional classifiers would. The flexibility of decision trees for handling input data in the form of continuous or categorical variables, and ancillary and/or missing data, and the improvements in accuracy shown with the use of ensemble classification techniques such as boosting (DeFries & Chan, 2000; Friedl et al., 1999) further supports their use. The benefits of decision trees have also been demonstrated with high-resolution multi-temporal Landsat ETM+ data (Brown de Colstoun et al., 2003). An excellent review of the methods used to construct decision trees is provided in Safavian and Landgrebe (1991). Friedl and Brodley (1997) discuss many of these methods within the context of research with remotely sensed data.

The current MODIS land cover algorithm inputs are 16-day composites for the individual MODIS land bands and the Enhanced Vegetation Index (EVI) (Huete et al., 2002) for an entire year. All the input data are adjusted to a nadir-viewing angle to reduce the effect of varying illumination and viewing geometries (Friedl et al., 2002). The use of temporal or phenological metrics describing the temporal evolution of the Normalized Difference Vegetation Index (NDVI) for various cover types was proposed by Lloyd (1990) as a means of resolving different cover types. DeFries et al. (1995, 1998) and Hansen et al. (2000) adopted the use of additional yearly metrics, including NDVI, obtained from the individual spectral bands of AVHRR. This provided greater information content and generally enhanced the separation of cover types which otherwise had similar NDVI. DeFries et al. (1998) tested 24 temporal metrics as input to their decision tree algorithm that were produced by extracting the yearly maximum and minimum for NDVI and the 5 AVHRR spectral bands, and calculating the yearly mean and amplitude (i.e. Max. – Min.). The yearly metrics provided significant data reduction while also ensuring that the training data from the northern and southern hemispheres had the same seasonal phase. It should be noted that land cover types exhibiting similar NDVI temporal signals, yet with different canopy architectures, will still be difficult to separate using only near-nadir signatures. Our goal here is to exploit the potentially unique land cover specific information contained in the BRDF to improve the separation of cover types which may otherwise be currently difficult to separate.

2.2. Exploitation of BRDF information

The BRDF of vegetation and soils reveals anisotropy that is spectrally, temporally, and spatially variable (Bicheron & Leroy, 2000; Brown de Colstoun et al., 1996; Deering et al., 1999; Irons et al., 1992; Kimes, 1983; Pinty et al., 2002; Walthall & Brown de Colstoun, 1997). Two processes are generally accepted to control the observed bidirectional signal of terrestrial surfaces (Roujean et al., 1992). The first is volume

scattering which describes the interaction of energy with a medium composed of facets oriented in many different directions such as leaves and/or soil particles. The second, geometric scattering, deals with the variability of the BRDF that is introduced by shadowing of scene components and by viewing different proportions of these components as the view angle of the sensor changes (Hapke et al., 1996; Kimes, 1983; Roujean et al., 1992).

Barnsley (1994), and particularly Barnsley et al. (1997), explored the information content and dimensionality of multiple view angle imagery by showing the potential for discriminating several agricultural cover types based on bidirectional information alone. Principal components analyses showed that, even with fairly limited data, the directional information appears to provide up to two more degrees of freedom for land cover separation beyond those available from nadir spectral data alone.

The coefficients of simple BRDF models such as those of Roujean et al. (1992) have been used in studies by Braswell et al. (1996), Roujean et al. (1997), and Walthall (1997), to show the potential of utilizing the angular signal described by the model coefficients to retrieve various biophysical surface parameters from AVHRR data, airborne BRDF data, and modeled values. Studies by Brown de Colstoun et al. (1996) and Walthall and Brown de Colstoun (1997) further suggest that the BRDF at the landscape level, as described by the three coefficients of the Walthall et al. (1985) model, may contain land cover specific information beyond the spectral domain of remote sensing which may be useful in discriminating land cover types. Wu et al. (1995) also showed bidirectional reflectance distributions to be strongly dependent on land cover at the regional scale. Bicheron and Leroy (2000) confirm from global POLDER data that the form of the BRDF for various cover types is different and that it varies with season. Finally, the enhanced discrimination and improvement in land cover classifications provided by bidirectional information has been demonstrated for sub-boreal and boreal land cover types by Abuelgasim et al. (1996) and Bicheron et al. (1997). The work of Bicheron et al. (1997) and Vanderbilt et al. (1997) showed that it is possible to discriminate wetlands from non-wetlands classes such as grasslands or forests using the strong specular reflection of water. Similarly, Leroy and Bréon (1996) found that rice paddies exhibit this same extreme anisotropy because of water and thus may be distinguishable from other crop types. Because of the vertical and geometric structure of buildings and other man-made structures, the BRDF may also provide information on urban and developed areas beyond what is available from near-nadir remote sensing.

Use of BRDF information may help improve the separation of classes that are currently difficult to separate. For example, in DeFries et al. (1995) and DeFries et al. (1998), land cover classes such as grasslands and croplands, woodlands and deciduous broadleaf forests, and closed bushland/shrublands and open shrublands have lower classification accuracies than most other classes because of substantial inter-class confusion. Land cover classes such as these which show similar spectral and/or temporal responses could be further distinguished by the

level of anisotropy they produce, as noted by Kriebel (1978), Kimes et al. (1985) and Pinty et al. (2002). Here, the height of tree canopies, and/or the degree of canopy closure, factors that modify the shadowing regime within each respective canopy, would again provide land cover information that could be measured from their BRDF. More open canopies would be expected to exhibit stronger anisotropy due to background or herbaceous layer reflectances than closed ones and this effect would be quantifiable in the shape of the BRDF. Finally, the use of BRDF information may further enhance classification of land cover classes that are already well characterized. This enhancement has already been shown for broadleaf, needleleaf, and other forested cover types (Abuelgasim et al., 1996; Bicheron et al., 1997).

3. Data and methods

The POLDER satellite system (Deschamps et al., 1994) can provide observations of a single target from up to 14 different directions during a single orbit. Over a month POLDER can provide, depending on latitude, measurements from 400+ different directions with good sampling along the principal plane of the sun and from a variety of azimuthal directions. The first POLDER instrument was launched in August 1996 onboard the Japanese Advanced Earth Observing Satellite (ADEOS-1) platform, with a 10:30 AM Equator crossing time. The ADEOS-1 spacecraft ceased to transmit at the end of June 1997, allowing only eight months of useable global coverage to be acquired, from about the end of October 1996 through June 1997. Our assessment of the eight-month NDVI data from POLDER showed that, with the exception of some areas at very high latitudes, the POLDER archive provided a nearly complete annual growth cycle for most of the globe.

3.1. POLDER instrument and data processing

The POLDER instrument uses a unique design based on a rectangular Charged Coupled Device (CCD) detector array, a rotating filter wheel carrying spectral and polarized filters, and a wide field of view lens (Bicheron & Leroy, 2000; Deschamps et al., 1994; Leroy et al., 1997). Through this lens, the field of view imaged by the CCD array is $\pm 43^\circ$ along track and $\pm 51^\circ$ across track (2200 km swath width), leading to view zenith angles of $\pm 50^\circ$ and $\pm 61^\circ$ in the along and cross track directions. The POLDER pixel is 6 by 7 km at nadir, growing by approximately 21% out to a viewing angle of 60° (Deschamps et al., 1994).

Multi-spectral images or ‘snapshots’ for 15 spectral bands are acquired every 19.6 s during one orbit, with substantial overlap between successive images along-track. This allows a particular point on the Earth to be observed from up to 14 different viewing directions during each satellite overpass. Successive orbits provide further looks of the same point from different azimuthal orientations, allowing a more complete sampling of the surface BRDF than available from other sensors such as AVHRR and/or MODIS.

Radiometrically corrected and geocoded top-of-atmosphere spectral reflectances for each image on an equal area sinusoidal

Earth grid, or ‘Level 1’ data, form the basis for the derivation of further POLDER products, such as ‘Level 2’ products processed for single POLDER orbits, and ‘Level 3’ global products, produced from multiple dates of POLDER acquisitions (Leroy et al., 1997). Within this data processing stream, the Level 1 data for the spectral bands centered at 443, 670, 765, 865 and 910 nm are screened for clouds, and corrections are applied for gaseous absorption, stratospheric aerosols, and Rayleigh scattering. Because the POLDER instrument does not carry thermal bands, the cloud screening is performed by using various tests aimed at detecting different types of clouds (Leroy et al., 1997). Even though tropospheric aerosols are retrieved directly from POLDER data, a correction for these aerosols was not yet implemented on these data because of varying confidence intervals of these retrievals (Leroy et al., 1997). Aerosol optical thickness estimates retrieved with sufficient confidence were used to screen pixels with very large aerosol loadings, or with optical thicknesses at 865 nm greater than 0.3.

The compositing of Level 2 single orbit data into 30-day global fields is not done using traditional maximum value compositing, as is typically done with AVHRR data, but rather by accumulating cloud-free atmospherically corrected surface reflectances that provide a sampling of the surface BRDF obtained from a multitude of viewing directions (Leroy et al., 1997). For periods of 30 days each centered on the 5th, 15th, and 25th day of each month, all cloud-free reflectances are used to derive bidirectional coefficients on a per-pixel basis. As described by Leroy et al. (1997), the objectives of this process are to obtain a sufficient number of observations for the Roujean et al. (1992) BRDF model to be properly fitted to the data, and also to reduce any errors introduced by sub-pixel clouds or improper cloud detection and/or atmospheric corrections. The derivation of the k_i coefficients of the Roujean et al. (1992) model (see Section 3.2 below) proceeds as follows: first, a linear regression of surface reflectances as a function of viewing angle is performed. Any retrieved surface reflectance whose distance from the regression line is greater than twice the root mean square error of the regression is discarded. Third, a second regression is performed using the remaining observations to derive the k_0 , k_1 , and k_2 coefficients of the Roujean et al. (1992) model. These coefficients are then used to calculate spectral hemispherical reflectances by integration over all view zenith and azimuth directions. The NDVI is calculated using the spectral hemispherical reflectances at 670 and 865 nm. For the research reported here, the entire eight-month archive of Level 3 NDVI, albedos and BRDF coefficients from POLDER was acquired directly from the CNES in Toulouse, France. Each global data layer was reprojected into a Goode’s Homolosine projection using software developed specifically for POLDER by the Laboratoire d’Optique Atmosphérique at the Université de Lille, France.

3.2. Roujean et al. (1992) BRDF model

The selection of a BRDF model for global applications is difficult because most BRDF models cannot always provide a

good statistical fit to all BRDF shapes while also providing a strong linkage with the guiding physical principles of radiative transfer. The choice of the Roujean et al. (1992) model for the research here was made because: (1) the coefficients have a physical basis for most surface types and BRDF patterns, (2) the model fits a wide variety of BRDF shapes and has been validated over both heterogeneous and homogeneous surfaces (Roujean et al., 1992), (3) the model can be fitted even when particular viewing directions may be missing, such as when clouds are present (Leroy & Roujean, 1994), (4) when integrated over the viewing hemisphere, the accuracies of the retrieved albedos are comparable or better than many of the other models (Privette et al., 1997). Other issues related to the ease of implementation at the global scale are also discussed by Leroy et al. (1997), particularly in terms of the global POLDER data processing system.

The Roujean et al. (1992) model was originally developed to correct satellite imagery for bidirectional effects. Working from the basic form of the Walthall et al. (1985) model, their original assumption was that the bidirectional reflectance of most terrestrial surfaces as a function of the solar zenith angle θ_s , view zenith angle θ_v , and relative azimuth angle ϕ , or $\rho(\theta_s, \theta_v, \phi)$, could be described by a linear combination of two analytic functions $f_1(\theta_s, \theta_v, \phi)$, and $f_2(\theta_s, \theta_v, \phi)$ such that:

$$\rho(\theta_s, \theta_v, \phi) = k_0 + k_1 f_1(\theta_s, \theta_v, \phi) + k_2 f_2(\theta_s, \theta_v, \phi), \quad (1)$$

where k_0 , k_1 , and k_2 are coefficients which describe the magnitude of the reflectance, and the importance of geometric and volume scattering effects, respectively.

The f_1 function, describing the geometric scattering component of the BRDF and the general contribution of shadowing to the BRDF shape, was modeled by assuming that the surface is covered with brick like protrusions with a length much larger than either their width or height. Roujean et al. (1992) described this function as:

$$f_1(\theta_s, \theta_v, \phi) = \frac{1}{2\pi} [(\pi - \phi)\cos\phi + \sin\phi]\tan\theta_s\tan\theta_v - \frac{1}{\pi} (\tan\theta_s + \tan\theta_v + \sqrt{\tan^2\theta_s + \tan^2\theta_v - 2\tan\theta_s\tan\theta_v\cos\phi}). \quad (2)$$

The volume scattering component, f_2 , was calculated from consideration of the radiative transfer of energy within a homogeneous turbid medium composed of randomly oriented facets such as leaves or soil particles. f_2 was defined as:

$$f_2(\theta_s, \theta_v, \phi) = \frac{4}{3\pi} \frac{1}{\cos\theta_s + \cos\theta_v} \left[\left(\frac{\pi}{2} - \xi \right) \cos\xi + \sin\xi \right] - \frac{1}{3}, \quad (3)$$

where ξ is the phase angle and is related to θ_s , θ_v and ϕ by:

$$\cos\xi = \cos\theta_s\cos\theta_v + \sin\theta_s\sin\theta_v\cos\phi. \quad (4)$$

The retrieval of the k_i coefficients is performed by regression between the measured reflectances and the modeled

reflectances calculated from Eqs. (1)–(3), with k_0 representing the reflectance at nadir with an overhead sun (Roujean et al., 1992).

By combining these two functions in Eq. (1), Roujean et al. (1992) were able to successfully fit their model to a wide variety of field measured BRDF surfaces from bare soils to densely vegetated canopies. Their analyses of 11 different land cover types showed that, in general, the k_2 coefficient was larger than the k_1 coefficient, indicating a dominance of volume scattering over geometric scattering effects for most cover types in both the red and near-infrared. Also, the general magnitude of both coefficients was larger for the near infrared than for the red portion of the electromagnetic spectrum, indicating a possible correlation of the retrieved coefficients with the spectral information. Finally, for some cover types, the retrieved k_1 coefficients were negative, and therefore ‘unphysical,’ according to Roujean et al. (1992). As is discussed in Leroy et al. (1997), the physics used by Roujean et al. (1992) did not adequately describe all possible surfaces, including those that exhibit specular reflection, and which may be one origin of the negative coefficients. However, in a purely statistical sense, the model will still fit the BRDF shapes appropriately in many cases, but the physical meaning of the coefficients may be lost or at least unclear. We found many negative model coefficients in the global POLDER data, particularly in areas with or near snow and/or water. Because the land cover classification algorithms are based primarily on statistical or pattern recognition principles, these negative coefficients were not considered particularly problematic for our analyses and could actually turn out to be beneficial to the classifications.

3.3. Global scale training data and derivation of BRDF metrics

The type of analysis we present here would have been impossible without the type of global scale training data we were able to utilize and which we co-registered to the global POLDER data. While global training sets are currently being developed and used as a part of the MODIS land cover product effort (Friedl et al., 2002), these are not yet available to the general public. The only currently available global training data set is that developed and used by DeFries et al. (1998) at 8 km spatial resolution, augmented by Hansen et al. (2000) for their 1 km land cover classification (<http://www.geog.umd.edu/landcover/global-cover.html>).

The process of deriving coarse scale training data has been described by DeFries et al. (1998) and Hansen et al. (2000). Their approach is based on the careful interpretation of over 150 Landsat Multi-Spectral Scanner (MSS) and TM imagery and then their co-registration to the 8 and 1 km AVHRR data. The Landsat scenes were selected in areas where three well-known classification products agreed that the cover type is present (DeFries & Townshend, 1994) and then re-projected into the Goode’s Interrupted Homolosine projection used by both the 8 km Pathfinder AVHRR Land (PAL) data (James & Kalluri, 1994) and the 1 km global AVHRR data (Eidenshink & Faundeen, 1994). The Landsat data were then co-registered

to both these global data sets by using a cross-correlation technique, where the highest degree of agreement between the NDVI of the Landsat data and the AVHRR data was found by “floating” the Landsat data over the AVHRR data (DeFries et al., 1998).

Large homogeneous areas with the land cover type of interest were delineated directly in each scene using ancillary data such as regional and local maps, and investigator knowledge of the area. For more heterogeneous areas, a supervised classification using a decision tree was used to identify the cover type of interest in the scene (DeFries et al., 1998; Hansen et al., 2000). These data were then ‘degraded’ to the spatial resolution of the AVHRR data sets. The identification of training pixels in the coarse scale data was made using the following rationale. For homogeneous scenes, if 100% of the pixels (90% in some rare cases) in the Landsat data were identified as the cover type on the coarse data then these were selected for training. For heterogeneous scenes, coarse pixels containing 90% (80% in rare cases) of the cover type identified in the Landsat data were selected. Hansen et al. (2000) extracted every fifth pixel from a full resolution 1 km training layer derived as above from pixels which contained 100% of the land cover type present in the Landsat data. The use of this reduced training set was due to the large data storage and computational requirements that were encountered when working with the full resolution 1 km global data.

Because the University of Maryland (UMD) training set did not contain the full set of classes as specified by the IGBP, we relabeled a small number of the training data from Hansen et al. (2000) into the IGBP Permanent Wetlands class (e.g. Everglades, Louisiana Swamps) (Brown de Colstoun, 2001). Other wetlands training data were delineated directly on the AVHRR data in regions with known large wetlands areas (e.g. Pantanal in Brazil, Okavango Delta in Africa, Russian wetlands east of the Urals). Urban areas were also delineated in this fashion for large urban complexes throughout the world (e.g. Los Angeles, Moscow, Beijing). Snow and ice training data were selected from large ice caps and/or glaciers in Greenland, Alaska, and Iceland. The IGBP Croplands/Natural Vegetation Mosaic class, which is problematic particularly in terms of poor accuracy (see Scepán, 1999), could have been modeled from a mixture of the other classes and/or specifically trained for during our analysis but we did not feel that a mosaic class at this spatial scale would necessarily add any new or interesting information to our analyses.

A set of 39,595 training pixels produced as described above for all IGBP classes except the Croplands/Natural Vegetation Mosaic class was then co-registered to the 6 by 7 km resolution POLDER data in the Goode’s projection, yielding a potential training set of 37,015 POLDER pixels at that resolution. The values of NDVI, spectral albedos for 443, 670, 765, and 865 nm, and the k_0 , k_1 , and k_2 coefficients for each band for each of these 37,015 pixels were extracted for each 30-day period in the eight-month archive. This entire data set was composed of 24 30-day periods for each parameter, for a total of 336 global layers, and provided a nearly complete annual growth cycle for most training pixels, with the exception of those at very high

latitudes. Out of the 37,015 training pixels, 367 were removed because they did not contain any retrievals over the entire measurement period. Table 1 shows the number of training pixels per IGBP land cover class for the remaining 36,648 pixels used for the analyses here.

The final step in the creation of the POLDER training data involved the development of metrics broadly describing the annual or temporal evolution of NDVI, spectral albedo, and the BRDF coefficients. For this, the maximum, minimum, mean and amplitude of each parameter over the eight-month record were extracted, as suggested by the work of DeFries et al. (1998). This was done both as a data reduction measure but also to ensure that training pixels for the same class in both the northern and southern hemispheres were in phase with each other. A total of 68 metrics were derived in this fashion from the 336 original layers with 20 metrics describing the NDVI and spectral albedo for the 443, 670, 765, and 865 nm bands. The metrics for the k_0 Roujean et al. (1992) model coefficient (nadir reflectance for overhead sun) for the four bands were not used because the spectral information was already present in the spectral albedo for the same four bands. Nonetheless, the 32 BRDF metrics for the k_1 and k_2 coefficients exemplify the large amount of potentially useful information provided by the BRDF in addition to the NDVI and spectral albedo information. These data were all used as input to the C5.0 classifier.

3.4. C5.0 decision tree classifier

The commercially available decision tree C5.0, the successor of the C4.5 program, (Quinlan, 1993) offered a tested, robust and state-of-the-art classifier with a simplicity in testing not duplicated with other classifiers. The use of boosting was also appealing from previous work with ensemble classifiers (Brown de Colstoun, 2001; Brown de Colstoun et al., 2000).

Decision tree classifiers successively partition the input data into more and more homogeneous subsets by producing

Table 1
Number of global training pixels used for POLDER classification analyses

IGBP class name	Number of training samples
1) Evergreen Needleleaf Forests (ENeF)	1663
2) Evergreen Broadleaf Forests (EBrF)	4316
3) Deciduous Needleleaf Forests (DNeF)	482
4) Deciduous Broadleaf Forest (DBrF)	1948
5) Mixed Forests (MixF)	1701
6) Closed Shrublands (ClSh)	1330
7) Open Shrublands (OpSh)	3011
8) Woody Savannas (WSav)	4016
9) Savannas (Savn)	1818
10) Grasslands (Gras)	3971
11) Permanent Wetlands (Wtld)	592
12) Croplands (Crop)	6482
13) Urban/Built-Up (Urbn)	201
15) Snow and Ice (Snow)	1489
16) Barren (Bare)	3628
TOTAL	36648

Note that IGBP Classes 14 (Croplands/Natural Vegetation Mosaic) and 17 (Water Bodies) have been omitted. Class abbreviations are used in other tables and figures in the text.

optimal rules which minimize the error rates in the branches of the tree (Safavian & Landgrebe, 1991; Weiss & Kulikowski, 1991). Typically, the tree finds decisions that fit nearly every case in the training data correctly (i.e. “overfitting”) and branches or leaves with higher error rates have to be ‘pruned’ back to produce a final output that is less complex yet has superior predictive capabilities (Quinlan, 1999). Each final leaf is then the result of following a set of mutually exclusive decision rules down the tree. C5.0 contains two automated methods for pruning based on user-specified parameters that describe the minimum number of cases that must follow each of the branches of a tree and/or the confidence level used to calculate the predicted error rate at each leaf, branch and/or sub-tree (Quinlan, 1993, 1999).

A series of classifiers such as decision trees, termed an ensemble, can also be combined to produce higher classification accuracies than any one of the particular classifiers. Ensemble classifier techniques such as boosting, where a series of decision trees is created in an iterative fashion with each successive tree focusing on the errors of the previous tree, or those instances that are most difficult to classify, and then produce a decision tree from majority voting, have been shown to produce improved results over standard decision trees (DeFries & Chan, 2000; Friedl et al., 1999).

The contribution of the additional BRDF data to global classifications was examined by running the C5.0 decision tree classifier using only the NDVI and albedo metrics as input in a first test, and then the NDVI, albedo, and BRDF coefficients in a second, and analyzing the differences in results for both data sets, both in terms of overall accuracy and per-class user’s and producer’s accuracies (Congalton & Green, 1999). The 36,648 training points were randomly divided into 20 equal-sized training and testing blocks, and C5.0 was run using a boosting mode and fairly severe pruning parameters determined from previous work with global AVHRR data (Brown de Colstoun, 2001). With this random training/testing technique, 50% of the data are used to generate a decision tree and the results are evaluated using the 50% testing samples that were kept separate from the tree-building process. This is repeated 20 times (i.e. number of train/test blocks). While this provides a somewhat optimistic estimate of the overall classifier accuracy, it does so for *all* tests carried out in our analyses, with and without the BRDF metrics. All results given below are averages and standard deviations in classification accuracies and/or errors for all 20 training and testing blocks.

4. Results and discussion

4.1. Analysis of global scale BRDF model coefficients

Fig. 1 shows a standard near-infrared color-composite for Australia generated from an accumulation of POLDER data over the month of November 1996. The evergreen forests near the coast in both southeast and northern Australia are clearly visible. Areas of Croplands to the southwest and southeast are also visible, as well as a large bright area with little or no vegetation in the center of the continent (Simpson Desert). A

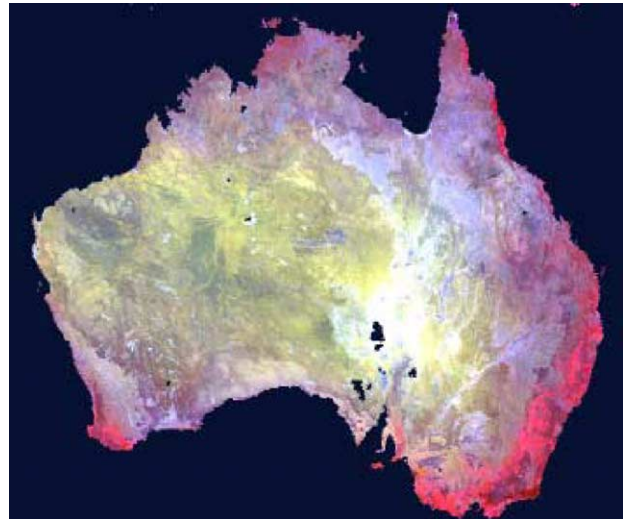


Fig. 1. Near-infrared color-composite image of Australia generated from POLDER data accumulated from November 1st to November 30th 1996. The k_0 coefficient of the Roujean et al. (1992) model POLDER bands at 865, 670 and 443 nm coded in red, green and blue, respectively.

large portion of the country, particularly trending towards the interior, contains Woodlands and Shrublands of varying tree densities and canopy cover, seen on Fig. 1 as shades of light red to yellow.

The data shown as Fig. 2 are from the same period as those used for Fig. 1 but in this case we have combined the k_0 , k_1 , and k_2 coefficients of the Roujean et al. (1992) model for the POLDER red band (670 nm) as red, green and blue. For Fig. 2, we find areas with more important volumetric effects at 670 nm in different shades of blue (e.g. dense broadleaf forests) while those with more important geometric effects (Woodlands and/or Shrublands) in shades of green and/or cyan. Subtle trends of geometric scattering possibly related to canopy density are also seen in the transition from the more densely forested east and southeast towards the interior Woodlands, and Shrublands and Grasslands.

The concept of combining BRDF model coefficients into color-composites is not new (Barnsley et al., 1997; Leroy et al., 1997). What we highlight here, particularly at the continental scale with the POLDER data, is how different the BRDF information is from more traditional information previously used for remotely sensed studies of land cover. Land cover patterns related to leaf chlorophyll, leaf area index, phenology, etc., are seen in Fig. 1 while in Fig. 2 we see a completely different perspective of Australia more in terms of canopy structure, geometry and density. While there are some correlations between the information in Figs. 1 and 2, and some of the land cover-specific information yet remains to be fully elucidated, these images do highlight the potential information that is available beyond the spectral domain, and which could be used for global land cover classifications.

Fig. 3a and b show the mean values for the ‘maximum k_1 ’ and ‘maximum k_2 ’ metrics for each IGBP land cover type and for the 670 and 865 nm POLDER bands. The large standard deviations for all classes are indicative of a rather large amount of overlap between all classes. However, it must be borne in

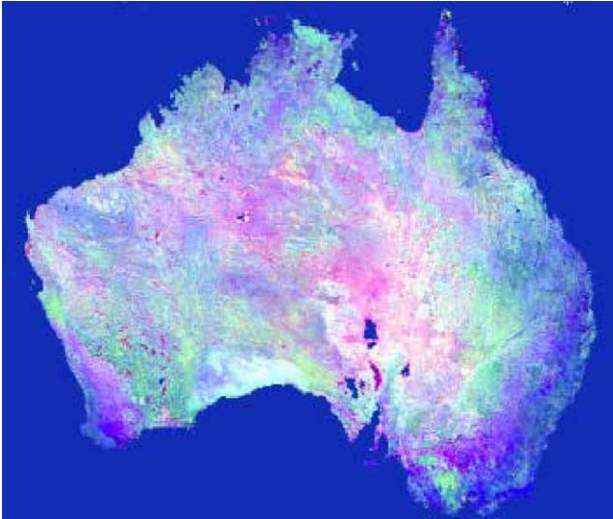


Fig. 2. Color composite from the same November 1996 POLDER data used for Fig. 1 but here the k_0 , k_1 , and k_2 coefficients of the Roujean et al. (1992) model for the POLDER red band (670 nm) are coded in red, green and blue. This image highlights the type of independent surface structure information available from BRDF coefficients.

mind that these training data are global, and as such are typically multi-modal in feature space, so that measures of central tendency are shown here to examine very broad patterns in the data. Moreover, a classifier such as a decision tree will be able to exploit areas of class overlap for classification as opposed to an MLC classifier which depends on per class statistics (Weiss & Kulikowski, 1991).

The coefficients for the 670 nm band presented as Fig. 3a generally show some larger values for the two shrublands and woodlands categories than for the forests classes, indicating that, as expected, the geometric scattering component is more important for these cover types. For this same coefficient, the Urban class also shows larger coefficients than the Bare category, implying that the geometric structure of this class may still be captured at this spatial scale. The k_1 coefficients for the near-infrared band are generally larger for forests than most other classes except Grasslands and Urban, indicating the relative importance of the shadowing effect for these dense canopies at this particular wavelength. It is interesting to note that the Wetlands category has generally smaller k_1 values than the other vegetated classes. Closer inspection of this class revealed many more negative coefficients than any other class, pointing out that the Roujean et al. (1992) could yield negative coefficients because of specular reflection. This same type of pattern was seen in many cases for the Snow category and is entirely consistent with the patterns observed for these classes by Bicheron and Leroy (2000) from global POLDER data. The large k_1 values found for the Grassland class for both bands run counter to expectations because the absence of trees and/or shrubs should decrease the geometric component of the BRDF in theory. From a classification standpoint, however, it is encouraging that the Grassland class shows different general patterns that either the Croplands or Wooded Grasslands categories because this may allow the confusion typically seen between these classes to be decreased.

The ‘maximum k_2 ’ metric for the 670 nm band shows no real trends across principal land cover core groups such as Forests, Woodlands and Shrublands, again with larger values being found on average for the Grasslands class. Larger values for this class are closer to expectations for this volumetric scattering parameter. For the 865 nm band, a decreasing trend with decreasing canopy density is apparent from the Evergreen Broadleaf Forests to the Woodlands, Wooded Grasslands, Closed Shrublands, Open Shrublands, and finally Bare classes. For these classes, this trend can be justified by the decreasing importance of volume scattering as the canopy density is decreased. Higher average values are found for the Grasslands, Croplands and Wetlands classes. For the first two classes, a higher volumetric scattering component is expected because these cover types have been typically modeled as turbid media (e.g. Verhoef, 1984). Higher values for the Wetlands category may be justified because these cover types are composed of water and either forests or grasses, and these cover types also show higher maximum k_2 values. Finally, smaller values found for the Evergreen and Deciduous Needleleaf Forest categories are attributed to the presence of snow because no

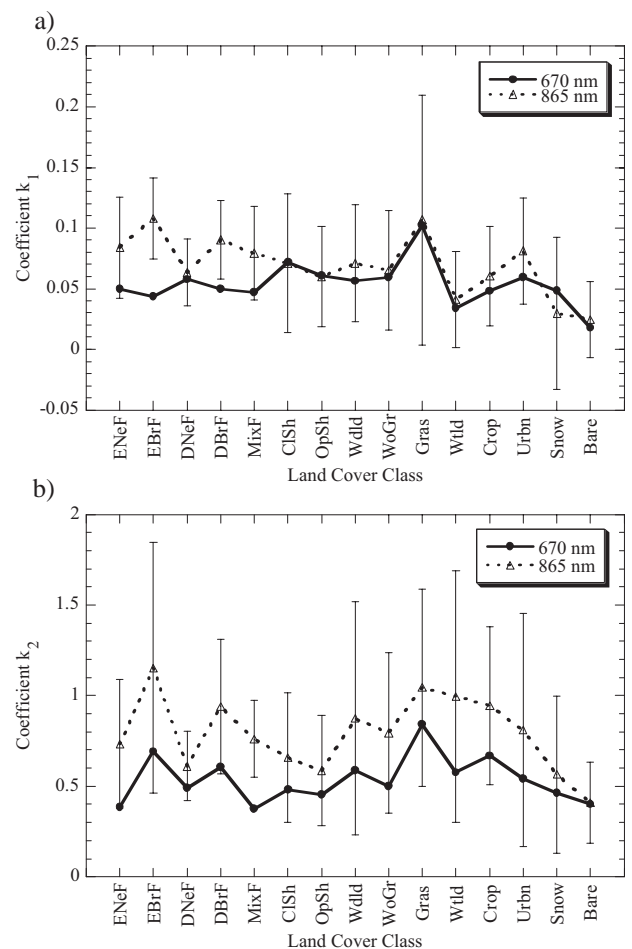


Fig. 3. Mean (a) k_1 and (b) k_2 coefficients for all training pixels in each of 15 IGBP land cover categories for POLDER bands at 670 and 865 nm. These are the averages for the maximum values for these coefficients over the 8-month POLDER record. Error bars represent ± 1 standard deviations. Only the error bars for 865 nm are shown for clarity and are similar to those at 670 nm.

attempt was made to mask out snow in the production of the metrics.

Examination of general statistics for all metrics, including NDVI, spectral albedos and BRDF coefficients, reveals general trends that are consistent with previously published data from field to global scales (Bicheron & Leroy, 2000; Roujean et al., 1992). The albedo and NDVI trends are consistent with expected patterns for vegetated, bare, and snow-covered terrestrial surfaces. For the BRDF metrics, the k_2 coefficients are much larger than the k_1 coefficients for all bands, as per Roujean et al. (1992), indicating a predominance of volume scattering effects on the observed BRDFs (Fig. 3). Both coefficients are typically larger in the near-infrared than the visible wavelengths, with the exception of the Snow class. Finally, the amplitude metrics for the coefficients indicate that, as expected, classes with greater inter-annual variability also show greater BRDF coefficient amplitudes.

The derivation of BRDF metrics from the POLDER data allows an examination of broad global scale bidirectional land cover patterns both spectrally and temporally. Fig. 4 illustrates the original concept of a bidirectional or ‘BRDF coefficient feature space’ from the POLDER data used for this analysis. The average ‘maximum k_1 ’ coefficient for the POLDER red band (670 nm) for each land cover class over the eight-month POLDER archive is plotted against the mean ‘maximum k_2 ’ coefficient for the 865 nm band, allowing an evaluation of heretofore unexplored patterns of remotely sensed data. Following the same general concepts of traditional red versus near infrared scatterplots for multi-spectral feature space, or maximum yearly NDVI versus mean annual NDVI for temporal feature space (DeFries et al., 1998), the BRDF feature space depicts the relationships between volumetric scattering (y axis on Fig. 4) and geometric scattering (x axis) for the different land cover types, and particularly as a function of surface structure. We note that, while there is substantial overlap between all classes in Fig. 4, these BRDF scatterplots still suggest that there are broad patterns related to surface structure and land cover in

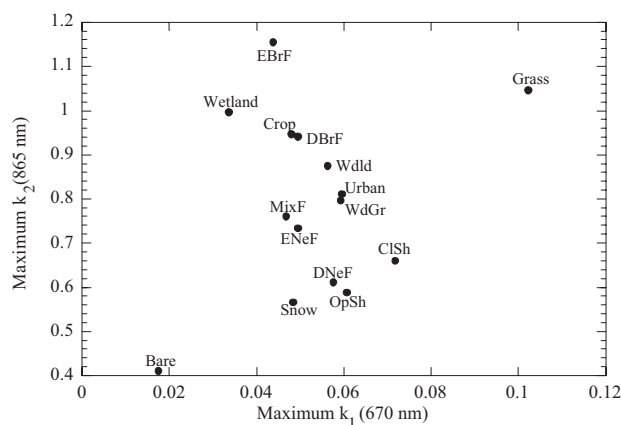


Fig. 4. Scatterplot introducing the concept of the ‘BRDF coefficient feature space’ from POLDER data. The mean ‘maximum k_1 ’ metric for the 670 nm POLDER band is plotted on the x axis with increasing geometric scattering effects from left to right. The mean ‘maximum k_2 ’ metric for the 865 nm POLDER band is plotted on the y axis, indicating larger volumetric scattering effects from bottom to top.

Table 2

Mean overall classification accuracies for 20 random training/testing blocks using POLDER data both with and without BRDF metrics

	50% training blocks	50% testing blocks
No BRDF (20 metrics)	91.20% (± 0.18)	81.90% (± 0.24)
BRDF (52 metrics)	95.31% (± 0.22)	85.05% (± 0.34)
Difference	4.11% (± 0.29)	3.15% (± 0.29)

Standard deviations for the 20 trees are shown in parentheses. Mean differences in classification accuracies for both methods are also shown.

the BRDF coefficients, and that this information is different from the information contained in either spectral or temporal feature space. The plots also indicate the potential for this information to aid the discrimination of particular cover types at the global scale. In particular, we note the potential for improved separation for classes such as Grasslands, Evergreen Broadleaf Forests, Wetlands, and Closed Shrublands based on their positions in BRDF feature space compared to other land cover classes. We should also note that we have plotted a red spectral band against a near-infrared band in Fig. 4 to highlight the fact that the BRDF space is also multi-spectral. Further, this BRDF space also varies seasonally implying that much work remains to fully understand all of the potential land cover information available in the surface BRDF. Of course, not all BRDF layers are expected to be independent from each other so the issues of the correlation of these additional data will also need to be further examined.

4.2. Classification of global scale POLDER data

The potential benefits of BRDF coefficients from POLDER for global land cover classifications were evaluated by running the C5.0 decision tree with only the NDVI and spectral albedo metrics, and then with these same metrics in addition to all 32 BRDF metrics. C5.0 was run in a boosted mode and results were examined for 20 different random samples of training and testing samples. Table 2 shows the mean accuracies for all 20 trees for each data set.

For the twenty 50% testing samples using only the NDVI and albedos, the overall accuracy is 81.90% (± 0.24) with a range of values from 81.40% to 82.40%. For these same metrics, the average accuracy for the 20 training samples is 91.20% (± 0.18), results whose mean values and stability agree quite well with those obtained with AVHRR data (Brown de Colstoun, 2001; DeFries et al., 1998).

When using the BRDF metrics with the other metrics, the mean accuracy for the testing samples improves to 85.05% (± 0.34), for a mean improvement of 3.15% (± 0.29). The accuracies for the testing samples range from 84% to 85.5%, with the mean differences between the two data sets ranging from a minimum of 2.6% to a maximum of 3.7%. The mean accuracy for the training sets is 95.31% (± 0.22), for a mean improvement of 4.11% (± 0.29).

While the gains in terms of overall classification accuracies are modest, considering that 32 additional layers were included in the BRDF classification, it is useful to examine these gains rather as a reduction of error or confusion of the classification.

Taking this point of view, the error reduction when using the BRDF metrics is 17%. It is also useful to examine the per class user's and producer's accuracies to determine whether particular classes may benefit more than others from the inclusion of the BRDF metrics. Tables 3 and 4 show the mean producer's and user's accuracies for the 20 trees, respectively.

Table 3 shows that the greatest increases of producer's accuracy are for the Grasslands class, with an 8.71% (± 1.03) improvement, the Wetlands class (8.02% ± 4.7), and the Urban class (7.82% ± 3.22). The increases seen for both the Wetlands and Urban classes, however, must be evaluated against much larger standard deviations, indicating that the results for these classes may not always be stable. Increases on the order of 4% to 5% are encountered for the Deciduous Broadleaf and Mixed Forest classes, the Closed Shrublands category, and the Woody Savanna class. For the mean user's accuracies, the largest mean increase is found for the Urban class but with a standard deviation greater than the mean value. Substantial improvement is seen in the user's accuracies for the Evergreen Needleleaf, Evergreen Broadleaf, Deciduous Broadleaf, and Mixed Forests classes, and the Woody Savannas and Wetlands classes, all with mean increases near, or greater than, 5%. These results indicate that the inclusion of BRDF coefficients in the classification can reduce the confusion between several land cover classes and thus improve both the user's and producer's accuracies. This improvement is seen across all land cover classes for the classifications performed here.

Closer examination of the error matrices for BRDF and non-BRDF classifications reveals that the principal differences between the two classification approaches are as follows: (1) there is much less confusion between all of the forest classes and the Woody Savanna class, and in particular between the Evergreen Broadleaf Forest class and the Woody Savanna class when using the BRDF coefficients. (2) There are some minor reductions in the confusion between the different forest classes, as well as between similar classes such as Closed and Open

Table 3
Mean producer's accuracies for 20 trees using no BRDF metrics and using 32 additional BRDF metrics from POLDER

IGBP class	Producer's accuracy		
	No BRDF	BRDF	Difference
1) ENeF	62.48% (± 1.31)	65.68% (± 1.73)	3.19% (± 1.69)
2) EBrF	93.81% (± 0.41)	96.54% (± 0.29)	2.73% (± 0.42)
3) DNeF	78.69% (± 2.97)	79.15% (± 2.77)	0.46% (± 3.59)
4) DBrF	76.11% (± 1.21)	79.56% (± 1.07)	3.46% (± 1.22)
5) MixF	63.43% (± 1.38)	67.53% (± 1.49)	4.10% (± 1.68)
6) ClSh	71.28% (± 3.01)	76.14% (± 2.32)	4.86% (± 2.50)
7) OpSh	90.20% (± 1.05)	91.28% (± 1.02)	1.08% (± 1.30)
8) WSav	71.51% (± 0.97)	77.37% (± 0.90)	5.85% (± 1.21)
9) Savn	52.26% (± 1.77)	54.36% (± 2.03)	2.10% (± 1.26)
10) Grass	76.01% (± 1.24)	84.73% (± 0.94)	8.71% (± 1.03)
11) Wtld	55.96% (± 3.19)	63.78% (± 2.48)	7.82% (± 3.22)
12) Crop	93.64% (± 0.54)	94.20% (± 0.58)	0.56% (± 0.55)
13) Urbn	31.54% (± 3.92)	39.55% (± 4.94)	8.02% (± 4.70)
15) Snow	98.31% (± 0.78)	98.64% (± 0.57)	0.33% (± 0.74)
16) Bare	97.91% (± 0.51)	98.48% (± 0.37)	0.57% (± 0.37)

Mean differences between the two data sets are also shown. Standard deviations for the 20 samples are given in parentheses for all mean values.

Table 4

Same as Table 3 but for mean user's accuracies

IGBP class	User's accuracy		
	No BRDF	BRDF	Difference
1) ENeF	68.43% (± 1.73)	74.00% (± 1.74)	5.57% (± 1.83)
2) EBrF	84.64% (± 0.75)	91.34% (± 0.66)	6.70% (± 1.22)
3) DNeF	74.88% (± 1.84)	75.15% (± 1.97)	0.27% (± 2.17)
4) DBrF	82.40% (± 0.94)	87.89% (± 1.26)	5.49% (± 1.28)
5) MixF	69.14% (± 1.60)	73.89% (± 1.51)	4.75% (± 1.85)
6) ClSh	82.74% (± 1.56)	84.24% (± 1.92)	1.50% (± 1.51)
7) OpSh	88.59% (± 1.17)	90.11% (± 0.90)	1.52% (± 1.37)
8) WSav	65.97% (± 1.29)	70.64% (± 0.93)	4.67% (± 1.15)
9) Savn	76.67% (± 1.90)	79.48% (± 2.18)	2.83% (± 2.37)
10) Grass	84.16% (± 0.86)	85.41% (± 1.08)	1.25% (± 1.41)
11) Wtld	74.93% (± 3.41)	80.04% (± 2.76)	5.12% (± 3.51)
12) Crop	83.53% (± 0.53)	85.84% (± 0.78)	2.30% (± 0.58)
13) Urbn	78.07% (± 7.04)	85.49% (± 5.95)	7.42% (± 7.83)
15) Snow	90.80% (± 2.17)	91.62% (± 1.00)	0.82% (± 1.70)
16) Bare	96.58% (± 0.63)	97.52% (± 0.59)	0.94% (± 0.37)

Shrublands. (3) There is a substantial reduction in the confusion between the Grasslands and Croplands classes. (4) The improvement for the Urban class is because of less confusion with the Croplands class but this represents a small number of pixels. Finally, the improvements seen for the Wetlands class come from a reduction in the confusion of this class with all of the different forest cover types. Smaller differences are found elsewhere.

5. Conclusions

The analyses conducted here indicate that the POLDER instrument provides the data required to study coarse BRDF patterns at the continental to global scales. Because of its unique sampling geometry, it is able to capture elements of the surface BRDF that are simply not available from cross-track scanners such as the AVHRR. The data from POLDER are also able to capture the broad features of the BRDF in multiple spectral bands and over time. Further, the eight-month archive of POLDER data is sufficient to allow the utilization of these seasonal BRDF patterns for the study of land cover.

The use of semi-empirical BRDF models (Roujean et al., 1992) with POLDER data allows the salient features of the surface BRDF for most cover types to be adequately described in an efficient manner, while retaining a physical meaning in most cases. The coefficients of the Roujean et al. (1992) model are able to describe the general importance of geometric and volumetric scattering effects for many cover types, with the broad patterns seen here concurring with patterns seen in field data and other global POLDER analyses (Bicheron & Leroy, 2000; Roujean et al., 1992). It is evident from the data analyzed here that the volumetric component of the BRDF is much more important than the geometric component for all cover types at this spatial scale. At the spatial scale of several kilometers of the POLDER global data, it is possible that the geometric structure of many canopies, such as trees and shrubs, and the shadowing that these features introduce, is much less important, and that the surface is much more of a turbid medium than at a finer scale. The broad variations seen in the k_1 coefficient

indicate that, even at this spatial scale, some information about the surface structure is still present.

The production of BRDF metrics from the POLDER data allows an investigation of the potential land cover specific information of the BRDF. This research finds that the patterns described by these metrics, even with a large amount of overlap between most classes, still contain information that is useful for land cover discrimination. By examining the feature space of the different BRDF metrics this information can be determined qualitatively. These ‘coefficient feature space’ plots indicate that the coarse scale BRDF coefficients from POLDER provide land cover information that is different from the spectral and temporal information, and is useful for land cover separation. Whether this information is actually completely independent from the spectral and temporal information is not yet known. Moreover, the actual independence of all the BRDF metrics from each other is an issue that merits further attention both in terms of potential data reduction but also future improvements.

Finally, the use of the POLDER BRDF metrics within a decision tree classifier shows that the metrics can reduce the overall errors of global land cover classifications. The metrics are shown to reduce the confusion between large core classes such as forests and Woody Savannas, for example. Further, the metrics can reduce the confusion between classes that show substantial confusion in spectral and temporal space such as Grasslands and Croplands, and increase the accuracy for such important classes such as Grasslands and Woody Savannas. The metrics also appear to contain information that allows a better classification of classes such as Wetlands and Urban areas. It is suggested that this approach may easily be applicable to multi-directional data currently available from MISR or future POLDER-like sensors. However, future analyses must attempt to better separate the variability introduced in the BRDF patterns by sensor and data processing errors from the natural inter- and intra-class variability of the BRDF for the different cover types. With potential improvements in the quality of the BRDF metrics used in the classification, it may be possible to provide improvements to global land cover accuracies beyond those seen here.

Acknowledgements

The authors would like to express their gratitude to Drs. John Townshend, Ruth DeFries and Matt Hansen from the Department of Geography at the University of Maryland for the provision of their global training data. The POLDER data was processed and made available by the Centre National d'Études Spatiales (CNES) in Toulouse, France. The MSPHINX software used to reproject the POLDER data was developed by L. Gonzalez and C. Deroo at the Laboratoire d'Optique Atmosphérique at the Université de Lille, France.

References

Abuelgasim, A. A., Gopal, S., Irons, J. R., & Strahler, A. H. (1996). Classification of ASAS multiangle and multispectral measurements using artificial neural networks. *Remote Sensing of Environment*, 57, 79–87.

Barnsley, M. J. (1994). Environmental monitoring using multiple-view-angle remotely-sensed data. In G. Foody, & P. Curran (Eds.), *Environmental remote sensing from regional to global scales* (pp. 181–201). Chichester: John Wiley and Sons.

Barnsley, M. J., Allison, D., & Lewis, P. (1997). On the information content of multiple view angle (MVA) images. *International Journal of Remote Sensing*, 18, 1937–1960.

Bicheron, P., & Leroy, M. (2000). Bidirectional reflectance distribution signatures of major biomes observed from space. *Journal of Geophysical Research*, 105, 26669–26681.

Bicheron, P., Leroy, M., Hauteceur, O., & Bréon, F. M. (1997). Enhanced discrimination of boreal forest covers with airborne directional POLDER data. *Journal of Geophysical Research*, 102, 29517–29528.

Bonan, G. (1997). Effects of land use on the climate of the United States. *Climatic Change*, 37, 449–486.

Braswell, B. H., Schimel, D. S., Privette, J. L., Moore III, B., Emery, W. J., Sulzman, E. W., et al. (1996). Extracting ecological and biophysical information from AVHRR optical data: An integrated algorithm based on inverse modeling. *Journal of Geophysical Research*, 101, 23335–23348.

Brown de Colstoun, E. C. (2001). *Automated Global Land Cover Classifications Using Satellite-Based Data From the Advanced Very High Resolution Radiometer (AVHRR) and Multi-Directional Data From the Polarized and Directionality Of Earth Reflectances (POLDER) Instrument*. Doctoral Dissertation, Department of Geography, University of Maryland, College Park, MD. 154 pp.

Brown de Colstoun, E. C., Story, M. H., Thompson, C., Commisso, K., Smith, T. G., & Irons, J. R. (2003). National park vegetation mapping using multi-temporal Landsat 7 data and a decision tree Classifier. *Remote Sensing of Environment*, 85, 316–327.

Brown de Colstoun, E. C., Walthall, C. L., Ciallella, A., Vermote, E. R., Halthore, R. N., & Irons, J. R. (1996). Variability of BRDF with land cover type for the West Central HAPEX-Sahel super site. *Proceedings of the 1996 International Geoscience and Remote Sensing Symposium (IGARSS'96)* (pp. 1904–1907). Piscataway, NJ: IEEE Geoscience and Remote Sensing Society.

Brown de Colstoun, E.C., Yang, W., DeFries, R., Hansen, M., and Townshend, J. (2000). *Surface Type Visible/Infrared Imager Radiometer Suite Algorithm Theoretical Basis Document, Version 3.0*. Available from World Wide Web site http://npoesslib.ipnoaa.gov/atbd_viirs.htm

Bounoua, L., DeFries, R. S., Collatz, G. J., Sellers, P., & Khan, H. (2002). Effects of land cover conversion on surface climate. *Climatic Change*, 52, 29–64.

Congalton, R. G., & Green, K. (1999). *Assessing the accuracy of remotely sensed data: Principles and practices*. Boca Raton, Fla: CRC Press.

Deering, D. W., Eck, T. F., & Banerjee, B. (1999). Characterization of the reflectance anisotropy of three boreal forest canopies in spring–summer. *Remote Sensing of Environment*, 67, 205–229.

DeFries, R. S., & Chan, J. C. W. (2000). Multiple criteria for evaluating machine learning algorithms for land cover classification from satellite data. *Remote Sensing of Environment*, 74, 503–515.

DeFries, R. S., Hansen, M., & Townshend, J. (1995). Global discrimination of land cover types from metrics derived from AVHRR pathfinder data. *Remote Sensing of Environment*, 54, 209–222.

DeFries, R. S., Hansen, M., Townshend, J. R. G., & Sohlberg, R. (1998). Global land cover classifications at 8 km spatial resolution: The use of training data derived from Landsat imagery in decision tree classifiers. *International Journal of Remote Sensing*, 19, 3141–3168.

DeFries, R. S., & Townshend, J. R. G. (1994). Global land cover: Comparison of ground-based data sets to classifications with AVHRR data. In G. Foody, & P. Curran (Eds.), *Environmental remote sensing from regional to global scales* (pp. 84–110). Chichester: John Wiley and Sons.

Deschamps, P. Y., Breon, F. M., Leroy, M., Podaire, A., Bricaud, A., Buriez, J. C., et al. (1994). The POLDER mission: Instrument characteristics and scientific objectives. *IEEE Transactions on Geoscience and Remote Sensing*, GE-32, 598–615.

Eidenshink, J. C., & Faundeen, J. L. (1994). The 1 km AVHRR global land data set: First stages in implementation. *International Journal of Remote Sensing*, 15, 3443–3462.

- Friedl, M. A., & Brodley, C. (1997). Decision tree classification of land cover from remotely sensed data. *Remote Sensing of Environment*, 61, 399–409.
- Friedl, M. A., Brodley, C. E., & Strahler, A. H. (1999). Maximizing land cover classification accuracies produced by decision trees at continental to global scales. *IEEE Transactions on Geoscience and Remote Sensing*, GE-37, 969–977.
- Friedl, M. A., Woodcock, C., Gopal, S., Muchoney, D., Strahler, A. H., & Barker-Schaaf, C. (2000). A note on procedures used for accuracy assessment in land cover maps derived from AVHRR data. *International Journal of Remote Sensing*, 21, 1073–1077.
- Friedl, M. A., McIver, D. K., Hodges, J. C. F., Zhang, X. Y., Muchoney, D., Strahler, A. H., et al. (2002). Global land cover mapping from MODIS: Algorithms and early results. *Remote Sensing of Environment*, 83, 287–302.
- Han, K. S., Champeaux, J. L., & Roujean, J. L. (2004). A land cover classification product over France at 1 km resolution using SPOT4-VEGETATION data. *Remote Sensing of Environment*, 92, 52–66.
- Hansen, M. C., DeFries, R. S., Townshend, J. R. G., & Sohlberg, R. (2000). Global land cover classification at 1 km spatial resolution using a classification tree approach. *International Journal of Remote Sensing*, 21, 1331–1364.
- Hansen, M., Dubayah, R., & DeFries, R. (1996). Classification trees: An alternative to traditional land cover classifiers. *International Journal of Remote Sensing*, 17, 1075–1081.
- Hansen, M., & Reed, B. (2000). A comparison of the IGBP-DIScover and the University of Maryland 1 km global land cover products. *International Journal of Remote Sensing*, 21, 1365–1374.
- Hapke, B., DiMucci, D., Nelson, R., & Smythe, W. (1996). The cause of the hot spot in vegetation canopies and soils: Shadow-hiding versus coherent backscatter. *Remote Sensing of Environment*, 58, 63–68.
- Huete, A., Didan, K., Miura, T., Rodriguez, E. P., Gao, X., & Ferreira, L. G. (2002). Overview of the radiometric and biophysical performance of the MODIS vegetation indices. *Remote Sensing of Environment*, 83, 185–213.
- Irons, J. R., Campbell, G. S., Norman, J. M., Graham, D. W., & Kovalick, W. M. (1992). Prediction and measurement of soil bidirectional reflectance. *IEEE Transactions on Geoscience and Remote Sensing*, GE-25, 372–383.
- James, M. E., & Kalluri, S. N. V. (1994). The pathfinder AVHRR land data set: An improved coarse resolution data set for terrestrial monitoring. *International Journal of Remote Sensing*, 15, 3347–3364.
- Kimes, D. S. (1983). Dynamics of directional reflectance factor distribution for vegetation canopies. *Applied Optics*, 22, 1364–1372.
- Kimes, D. S., Newcomb, W. W., Tucker, C., Zonneveld, I., Van Wijngaarden, W., de Leeuw, J., et al. (1985). Directional reflectance factor distributions for cover types of northern Africa. *Remote Sensing of Environment*, 18, 1–19.
- Kriebel, K. T. (1978). Measured spectral bidirectional reflection properties of four vegetated surfaces. *Applied Optics*, 17, 253–259.
- Leroy, M., & Bréon, F. M. (1996). Angular signatures of surface reflectances from airborne POLDER data. *Remote Sensing of Environment*, 57, 97–107.
- Leroy, M., & Roujean, J. -L. (1994). Sun and view angle corrections on reflectances derived from NOAA/AVHRR data. *IEEE Transactions on Geoscience and Remote Sensing*, 32, 684–697.
- Leroy, M., Deuzé, F. -M., Bréon, O., Hauteceur, M., Herman, J. -C., Buriez, D., et al. (1997). Retrieval of atmospheric properties and surface bidirectional reflectances over land from POLDER/ADEOS. *Journal of Geophysical Research*, 102, 17023–17037.
- Lloyd, D. (1990). A phenological classification of terrestrial vegetation using shortwave vegetation index imagery. *International Journal of Remote Sensing*, 11, 2269–2279.
- Loveland, T. R., & Belward, A. S. (1997). The IGBP-DIS global 1 km land cover data set, DISCover: First results. *International Journal of Remote Sensing*, 18, 3289–3295.
- Loveland, T. R., et al. (1999). An analysis of the IGBP global land-cover characterization process. *Photogrammetric Engineering and Remote Sensing*, 65, 1021–1032.
- Pinty, B., Widlowksi, J. -L., Gobron, N., Verstraete, M. M., & Diner, D. J. (2002). Uniqueness of multiangular measurements: Part I. An indicator of subpixel surface heterogeneity from MISR. *IEEE Transactions on Geoscience and Remote Sensing*, 40, 1560–1573.
- Privette, J. L., Eck, T. F., & Deering, D. W. (1997). Estimating spectral albedo and nadir reflectance through inversion of simple BRDF models with AVHRR/MODIS-like data. *Journal of Geophysical Research*, 102, 29529–29542.
- Quinlan, J. R. (1993). *C4.5: Programs for machine learning*. San Mateo, CA: Morgan Kaufman Publishers, Inc.
- Quinlan, J. R. (1999). Simplifying decision trees. *International Journal of human-computer Studies*, 51, 497–510.
- Roujean, J. L., Latoy, M., & Deschamps, P. Y. (1992). A bidirectional reflectance model of the earths surface for the correction of remote sensing data. *Journal of Geophysical Research*, 97, 20455–20468.
- Roujean, J. L., Tanré, D., Bréon, F. M., & Deuzé, J. L. (1997). Retrieval of land surface parameters from airborne POLDER BRDF during HAPEX-Sahel. *Journal of Geophysical Research*, 102, 11201–11218.
- Safavian, S. R., & Landgrebe, D. (1991). A survey of decision tree classifier methodology. *IEEE Transactions on Systems, Man, and Cybernetics*, 21, 660–674.
- Scepan, J. (1999). Thematic validation of high-resolution global land-cover data sets. *Photogrammetric Engineering and Remote Sensing*, 65, 1051–1060.
- Sellers, P. J., Los, S. O., Tucker, C. J., Justice, C. O., Dazlich, D. A., Collatz, G. J., et al. (1996). A revised land surface parameterization (SiB2) for atmospheric GCMs: Part II. The generation of global fields of terrestrial biophysical parameters from satellite data. *Journal of Climate*, 9, 706–737.
- Strahler, A.H. et al. (1999). *MODIS Land Cover Product: Algorithm Theoretical Basis Document, Version 5.0*. Available from World Wide Web Site: <http://sps0.gsfc.nasa.gov/atbd/modistables.html>
- Townshend, J. R. G., Justice, C. O., Skole, D., Malingreau, J. -P., Cihlar, J., Teillet, P., et al. (1994). The 1 km resolution global data set: Needs of the International Geosphere Biosphere Programme. *International Journal of Remote Sensing*, 15, 3417–3442.
- Vanderbilt, V. C., Perry, G. L., Steam, J. A., Ustin, S. L., Diaz Barrios, M. C., Zedler, S., et al. (1997). Discrimination of wetland and non-wetland community types with multi-spectral, multi-angle, polarized POLDER data. In G. Guyot & T. Phulpin (Eds.), *Proceedings of the Seventh International Symposium on Physical Measurements and Signatures in Remote Sensing* (pp. 47–49). Courchevel, France, London: Taylor and Francis.
- Verhoef, W. (1984). Light scattering by leaf layers with application to canopy reflectance modeling: The SAIL model. *Remote Sensing of Environment*, 16, 125–141.
- Walthall, C. L. (1997). A study of reflectance anisotropy and canopy structure. *Remote Sensing of Environment*, 61, 118–128.
- Walthall, C. L. & Brown de Colstoun, E. C. (1997). Medium altitude bidirectional imaging spectroradiometer measurements over the HAPEX-Sahel west central super site using the advanced solid-state array spectroradiometer (ASAS), In P., Kabat, S. D., Prince & L., Prihodko (Eds.), *HAPEX Sahel west central supersite: Methods, measurements and selected results*, Report 130, DLO Winand Staring Centre, Wageningen, The Netherlands.
- Walthall, C. L., Norman, J. M., Welles, J. M., Campbell, G., & Blad, B. L. (1985). Simple equation to approximate the bidirectional reflectance from vegetative canopies and bare soil surfaces. *Applied Optics*, 14, 383–387.
- Weiss, S. M., & Kulikowski, C. A. (1991). *Computer systems that learn*. San Mateo: Morgan Kaufman Publishers.
- Wu, A., Li, Z., & Cihlar, J. (1995). Effects of land cover type and greenness on advanced very high resolution radiometer bidirectional reflectances: Analysis and removal. *Journal of Geophysical Research*, 100, 9179–9192.